Title

Mechanism of CO2 Photocatalytic Reduction to Methane and Methanol on Defected Anatase TiO2 (101): A Density Functional Theory Study

Journal

The Journal of Physical Chemistry C, 123(6)

ISSN

1932-7447

Authors

Liu, Ji-Yuan
Gong, Xue-Qing
Alexandrova, Anastassia N

Publication Date

2019-02-14

DOI

10.1021/acs.jpcc.8b09539

Peer reviewed

Mechanism of CO_2 Photocatalytic Reduction to Methane and Methanol on Defected Anatase TiO_2 (101): A DFT Study

Ji-Yuan Liu[1,2], Xue-Qing Gong[2] and Anastassia Alexandrova[1,3,*]

[1]*Department of Chemistry and Biochemistry, University of California, Los Angeles, Los Angeles, CA, 90095, USA*

[2]*Key Laboratory for Advanced Materials, Center for Computational Chemistry and Research Institute of Industrial Catalysis, School of Chemistry and Molecular Engineering, East China University of Science and Technology, 130 Meilong Road, Shanghai 200237, P. R. China.*

[3]*California NanoSystems Institute, Los Angeles, CA, 90095, USA*

Corresponding Author e-mail: ana@chem.ucla.edu

ABSTRACT: With rising emission of CO_2 affecting human life, photocatalytic reduction of CO_2 attracts substantial research interest. Anatase TiO_2 is known to be one of the most promising catalysts of this process. Here, we adopted density functional theory calculations to systematically study the pathways of CO_2 reduction on the defected anatase TiO_2(101) surface. We find that oxygen vacancies play a critical role in promoting the reaction, as compared to the pristine surface. They help CO_2 binding, activation, and dissociation, and stabilize other reaction intermediates. The most feasible identified reaction mechanism proceeds through surface CO species, to CHO, CHOH, CH_2OH or CHO, CH_2O, and CH_3O, to produce methane and methanol. In addition, there exists a carbene-like deoxygenation pathway to form the CH species on the vacancy, which can give rise to methane by binding protons successively.

Introduction

Carbon dioxide, mainly emitted from human activities, *e.g.*, the combustion of fossil fuels, is a putative cause of the global warming. To reduce carbon dioxide, many methods such as photocatalytic, electrocatalytic, photoelectrocatalytic reduction, thermoreduction etc. have been widely studied recently.[1–9] Among the ways of conversion of CO_2, the most attractive one is to use the solar energy and photocatalytically convert CO_2 back to usable organic fuels, such as methanol. Photocatalysis consists of three steps: the solar light harvesting process, the separation and transport of photogenerated electrons and holes, and the reactions at the surface. Photoelectrocatalysis is a powerful technique that has advantages as compared to both photocatalysis, and electrocatalysis. On the one hand, the solar energy consumed in the process can significantly reduce the applied potential, and thus decrease the consumption of electricity. On the other hand, the applied electric potential can help photo-induced electron-hole pair separation, causing the hole migration to the anode where it can participate in the oxidation reaction. Although photo- and photoelectro-catalytic reactions occur in different chemical conditions, the charge transfer mechanism that underlies them is similar and consists of transferring electrons to the reactants through the catalyst to facilitate the conversion. However, the details of this mechanism for CO_2 conversion still remain unclear. Therefore, in this paper, we focus on the reaction mechanism in photocatalytic reduction of CO_2, with the goal of providing an insight into the mechanisms of both photocatalytic and photoelectrocatalytic reduction.

The pioneering study was led by Inoue et al in 1979, first finding that CO_2 could be reduced at the surfaces of several semiconductors, such as titanium

dioxide (TiO_2), under illumination.[10] TiO_2 has charming properties such as low cost, stability, and a large band gap, and is widely studied experimentally and theoretically for the CO_2 reduction.[11–20] TiO_2 has three common phases, rutile, anatase, and brookite.[21] Among these phases, rutile and anatase are investigated most widely investigated. Additionally, because the rate of electron-hole recombination in anatase (101) is more than 10 times smaller than in rutile (110)[22], the anatase phase has a better performance in the photo-driven charge transfer system. The anatase phase of TiO_2 has two common facets, (001) and (101), where the (101) is the thermodynamically most stable one[23]. Yu et al[13] suggested that the (101) facet should be the reactive surface in photocatalytic reactions because it has a lower conduction band edge. The (001) facet can trap holes and transfer electrons to the (101) surface, to prepare its reduced state for the reduction of CO_2. Therefore, anatase TiO_2 (101) is considered the reactive surface through this study.

Over recent years, the reduction of CO_2 to methane and methanol on pristine anatase TiO_2 has been widely investigated theoretically. He et al. was the first one who calculated the conversion of CO_2 to HCOOH on titania, and claimed a two-electron mechanism of the formation of formic acid from carbon dioxide.[15,16] The study by Ji et al. followed this direction, extending the results to the formation of CH_4 and CH_3OH, and verified the importance of oxygen vacancy on the surface.[19,20] Ip et al. analyzed the probabilities of carbene, formaldehyde, and glyoxal pathways suggested by experiment.[18]

Indeed, anatase is highly prone to having defects, such as oxygen vacancies, O_v, as well as forming amorphous structures. It was furthermore shown that the presence of O_v is essential for explaining the activity of anatase in photocatalytic applications.[24,25] Even though Ji et al already studied some parts of the pathway working on defective surface, there are still blanks remaining, and the present study fills some of them.

In our work, the photocatalytic process of CO_2 reduction on the (101) facet of anatase TiO_2 with an oxygen vacancy, was simulated. One hydrogen atom was introduced into the system at each photocatalytic step. The electron from adsorbed hydrogen atom can spontaneously move to surface producing a proton and an electron in the surface, as proved by both theory[26] and experiment[27]. Hence, the introduced hydrogen can be separated into H^+ and e^- participating in consecutive reaction steps. Because no experimental evidence of multielectron-transfer process was found for photocatalysis on semiconductors,[28] and also, one electron step has been reported before[11], we investigated the pathways proceeding through one-electron process, based on Scheme 1, where solid arrows represent hydrogenation steps.

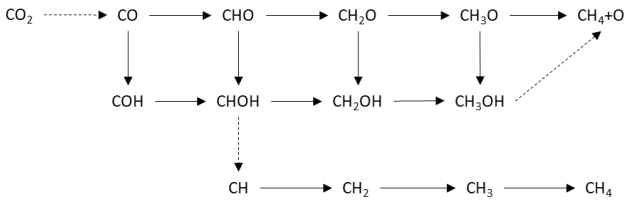

Scheme 1. Perspective pathway from CO_2 to CH_4/CH_3OH. Solid arrows represent hydrogenation step, while dash arrow represents a reduction step.

Computational Details

All DFT+U calculations were performed with the Vienna Ab initio Simulation Package (VASP). [29–32] The projector augment wave (PAW)[33,34] method with the Perdew, Burke and Ernzerhof (PBE)[35] functional was used to optimize the lattice parameters and relax the structures. A 400 eV plane-wave cut-off energy and spin polarization were set, and the residual force components on

each atom were lower than 0.03 eV·Å^{-1}·atom^{-1}. The Tkatchenko-Scheffler dispersion correction method[36] was adopted. The effective parameter of coulomb interaction correction of Ti atoms, U_{eff}, was set as 3.5 eV, which has been studied in our previous work.[37] The k-mesh of 2 x 2 was utilized. Bader charge analysis was considered on adsorption configurations.[38] The climbing image nudged elastic band (cNEB) method was utilized for transition state search.[39] All the transition state geometries were confirmed by phonon calculations, and each had just one imaginary mode aligned with the reaction coordinate.

The surface slab was made by cleaving a (3 × 1) supercell of optimized anatase TiO_2 bulk as a (101) surface, with an oxygen atom removed from the middle of top layer, as shown in Figure 1. The best number of layers was tested as shown in Table S1. It converged at four O-Ti-O layers with the bottom two layers frozen. The vacuum layer was 15 Å thick. In our earlier study[37], as well as in the recent paper by Ko et al[40], it was shown that a fairly large unit cell, as well as the carefully chosen level of theory (the DFT functional, Hubbard U correction, and inclusion of dispersion) are required to produce meaningful results for defected anatase.

All the adsorption and desorption energies were calculated by using the following formula:

$$E_{ads} = -E_{des} = E(adsorbate@slab) - E(slab) - E(adsorbate)$$

Where E stands for DFT+U calculated energy in eV, and E_{ads}, E_{des} are energies of adsorption and desorption, respectively.

During the specific illumination on TiO_2, electron-hole pairs keep being separated and recombining. Holes combine with water molecules to produce protons, hydroxyl groups, and oxygen, while electrons and protons generated from the holes take part in the reduction reaction. Because reactions are multi-step, to align the energy with different number of protons and electrons, the following formula was used:

$$E'_{state} = E_{state} - n(H) \bullet E_{ads}(H)$$

Where E_{state}, E'_{state} are the original and aligned energies of a same state (initial, transition, intermediate, or final), respectively, and n(H) is the number of hydrogen atoms in that state. $E_{ads}(H)$ represents for the energy of single hydrogen atom adsorbed on the oxygen defective (101) slab. All the energies of reaction states are shown as E'_{state}. The absolute aligned energy differences between with and without new introduced hydrogen atom of the same configuration are within 0.08 eV. There is only one exception and we will discuss it in the section C Pathway.

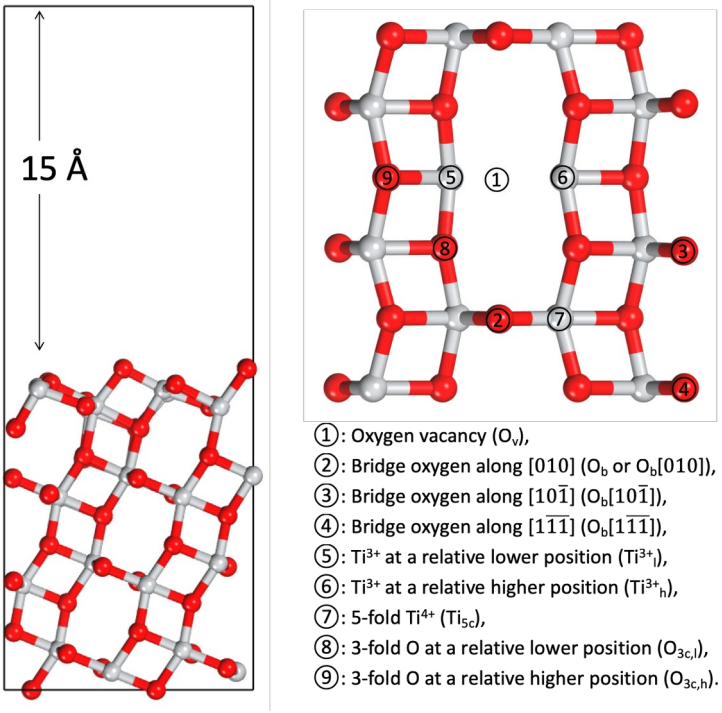

Figure 1. The side (left) and top (right) view of the anatase TiO_2 (101) surface slab. The silver and red spheres represent the Ti and O, respectively. O_v, O_b, O_b[010], O_b[$10\acute{1}$], O_b[$1\acute{1}1$], Ti^{3+}_l, Ti^{3+}_h, Ti_{5c}, $O_{3c,l}$ and $O_{3c,h}$ are illustrated respectively.

Results & discussion

Adsorption and dissociation of CO_2 reduction

When adsorbing on anatase, the CO_2 molecule bends, and binds to the O_v either "horizontally" as a CO_2(H) site with an adsorption energy of -0.89 eV (Figure 2a), or "vertically", occupying the vacancy as a CO_2(V) with an adsorption energy of -0.65 eV, as shown in Figure 2b. Both adsorption energies are larger than that corresponding to the most stable configuration of CO_2 on the pristine anatase (101) surface (-0.45 eV) (Figure S1). This suggests that CO_2 likely occupies the vacancy site. Charge transfer approves this result as well. It shows that in CO_2(H), CO_2 molecule accepts 0.84 e from surface slab, in which 0.76 e was distributed to C and 0.38 e was contributed by Ti^{3+} around the vacancy, while in CO_2(V), CO_2 accepts a little bit less electron of 0.83 e, in which 0.40 e was contributed by Ti^{3+} and 0.73 e was distributed to C. It's obvious that rather than O atom, the transferred electrons prefer to be localized on C atom. Moreover, it seems CO_2 becomes more stable when C receives more electron. This could be attributed to extra electrons make CO_2 bend easily and stable. Charge density plots (Figure S2a for CO_2(H) and S2b for CO_2(V)) illustrate the transition metal's d orbits play an important role in activating CO_2 molecules. From the computed potential surface (Figure 2c) and transition states (Figure S3), we find that CO_2(H) needs to overcome a significant barrier of 0.74 eV to transform to CO_2(V). Meanwhile, a similar activation energy of 0.76 eV is required to form CO; note that our number is a little bit higher than the barrier previously reported by Sorescu et al.,[41] likely because we computed a single step reaction from CO_2(H) to CO, whereas it is a two-step process in their work. From CO_2(V), only 0.15 eV activation energy is needed to form CO, which is quite a bit lower

than that from CO_2(H). Both pathways cure the O_v, consistently with the experimental work.[12]

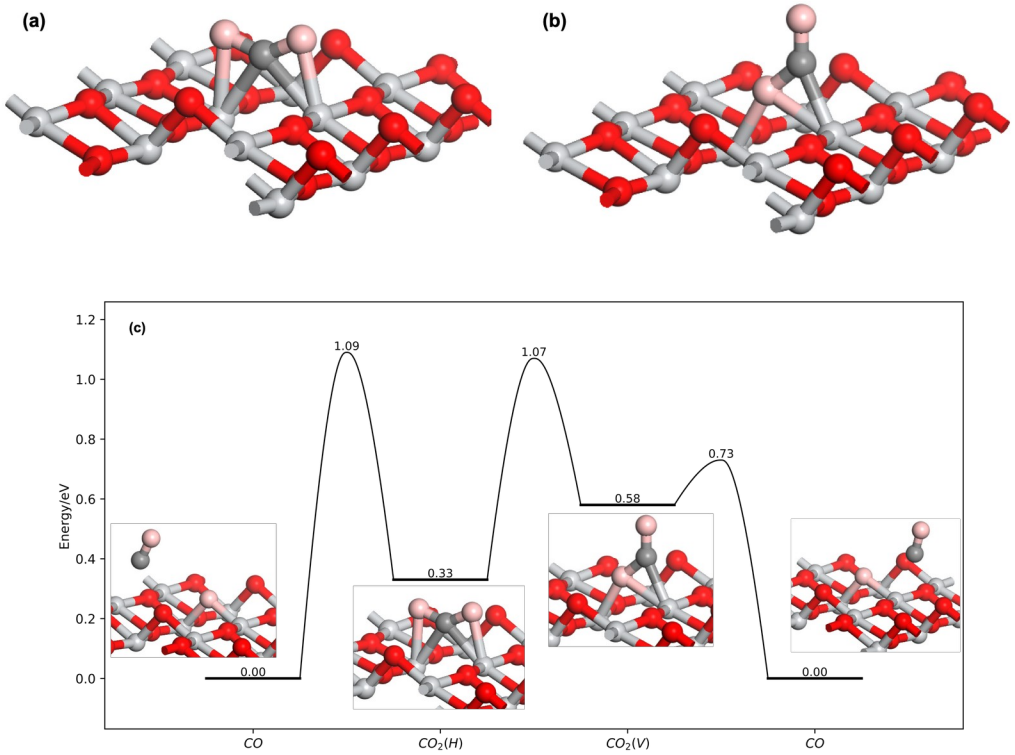

Figure 2. Configurations of adsorbed CO_2 on O_v site: (a): CO_2(H); (b): CO_2(V). (c): Adsorption and dissociation of CO_2 on the oxygen vacancy site. The silver, red, pink and grey spheres represent the Ti, O, O in CO_2 and C, respectively.

Adsorption of hydrogen on pristine and defected anatase TiO_2 (101) surface

The adsorption of hydrogen, the electron and proton source, was also studied before introduced into the system. For pristine slab, there are three different sites to activate hydrogen for binding, O_b, $O_{3c,h}$ and $O_{3c,l}$. Based on bader charge analysis, the average localized electrons on $O_{3c,h}$ is 0.018 more than $O_{3c,l}$, and the $E_{ads}(H)$ on $O_{3c,h}$ is accordingly less stable of 0.11 eV than $O_{3c,l}$ (shown in Table 1), otherwise the electron on hydrogen cannot be transferred to the surface. The hydrogen average binding energy is -2.68 eV on the O_b, which is far more stable than those on O_{3c}. In terms of the defected surface, more sites such as the O_b along different directions need to be considered. The average $E_{ads}(H)$ on different O_b and O_{3c} are rather close to those on pristine slab. Interestingly, Ti^{3+} could be another new anchor point for atomic hydrogen binding on, with an adsorption energy of -2.72 eV, which is at a similar level as O_b. Therefore, hydrogen would like to evenly diffuse to each O_b and Ti^{3+} sites and $O_b[010]$ is reasonably set as a mount point for introducing hydrogen.

Table 1. The adsorption of hydrogen on pristine and defected anatase TiO_2 (101) surface slab.

Adsorption site	Adsorption energy/eV
O_b@pristine	-2.68[a]

$O_{3c,\,h}$@pristine	-1.88
$O_{3h,\,l}$@pristine	-1.98
Ti_{5c}@pristine	N/A
$O_b[010]$@defected	-2.65[a]
$O_b[10\acute{1}]$@defected	-2.69[a]
$O_b[11\acute{1}]$@defected	-2.62[a]
$O_{3c,\,h}$@defected	-1.89
$O_{3c,\,l}$@defected	-2.00
$Ti^{3+}{}_h$@defected	-2.42
$Ti^{3+}{}_l$@defected	-2.72

a: All energies marked with a superscript '*a*' represent an average energy among a few similar configurations.

Adsorption of CO on oxygen vacancy

The pathways of HCOOH being obtained from CO_2 or CO on pristine anatase surface have been investigated before[16,19] and CO was reported[19] cannot bind to the pristine surface, hence, we focused on the role of O_v in the reduction reaction. Since only a part of catalytic cycle was investigated in this article, the recovery of O_v would not be discussed. The adsorption of CO on O_v site is shown in Figure 3a and 3b. There are two initial adsorption configurations. The one, named CO(A), has only the C atom binding to Ti^{3+}, and it is more stable, with the adsorption energy of -0.97 eV. The configuration called CO(B), features the bidentate binding to the surface and has a smaller adsorption energy of -0.48 eV. We can see that the CO(A) configuration has a stronger adsorption to anatase (101) than CO_2(H), suggesting that CO is going to strongly compete with CO_2 binding to the O_v site. Charge analysis also supported this. C gains 0.38 e in CO(A) and 0.37 e in CO(B), respectively. Besides, the length of C-O and C-Ti in CO(A) are 1.16 and 2.18 Å, which are shorter than corresponding bond lengths in CO(B) as 1.18 and 2.32 Å, suggesting the adsorption of CO(A) is more stable.

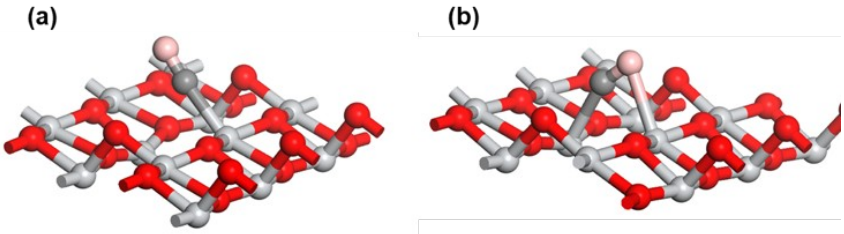

Figure 3. Adsorption of CO on the oxygen vacancy site. (a) the more stable monodentate configuration CO(A) with C binding to Ti^{3+}; (b) the less stable bidentate configuration CO(B). The silver, red, pink and grey spheres represent the Ti, O, O in CO and C, respectively.

Hydrogenation was studied from these two initial points separately. As described before, only one hydrogen atom was introduced into the system per reaction step and adsorbed on the O_b site to the participate in the photocatalytic reduction.

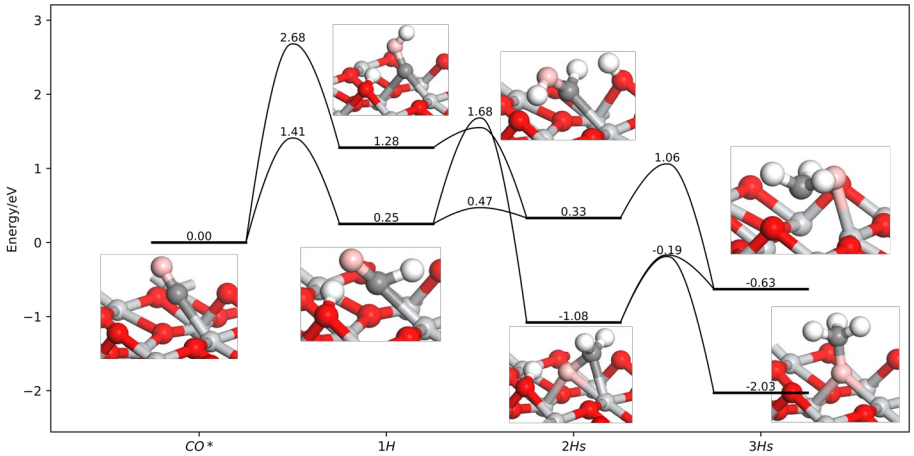

Figure 4. The computed reaction pathway starting from configuration CO(A) and yielding the methyl species bound to the surface. The CO*[*n*H(s)] labels on x-axis represents the configurations in this column contain extra adsorbed CO [*n* hydrogen atom(s)].

First, we consider the reduction of CO by binding H^+ starting from the configuration CO(A) (Figure 4). The barrier to binding H^+ to O in CO is much higher than that to binding H to C. It is not surprising, because the oxygen atom in CO(A) is far away from the O_b site holding H^+, and thus proton binding must proceed through an energetically-costly radical mechanism, shown in Figure S5. The total energy of the forming COH species is higher than that of CHO, suggesting that CHO might be the main product in the first hydrogenated step starting from CO(A). In the second step, regardless of the intermediate formed in the first step from which the reaction begins, the CHOH intermediate forms preferentially over CH_2O, even though CH_2O is much more stable. The barrier is only 0.22 eV to hydrogenate CHO to CHOH, while the barrier to form CH_2O is 1.43 eV, which is greater than the total barrier of 0.81 eV to hydrogenate CHO to the CH_2OH intermediate. Additionally, although the pathways of CHOH → CH_2OH and CH_2O → CH_3 are both exothermic, the barriers to the former (0.73 eV) is smaller than that to the latter (0.89 eV). This suggests that CH_2OH is a more favorable intermediate to form along the pathway starting from the configuration CO(A), with the rate determining step being the first hydrogenated step.

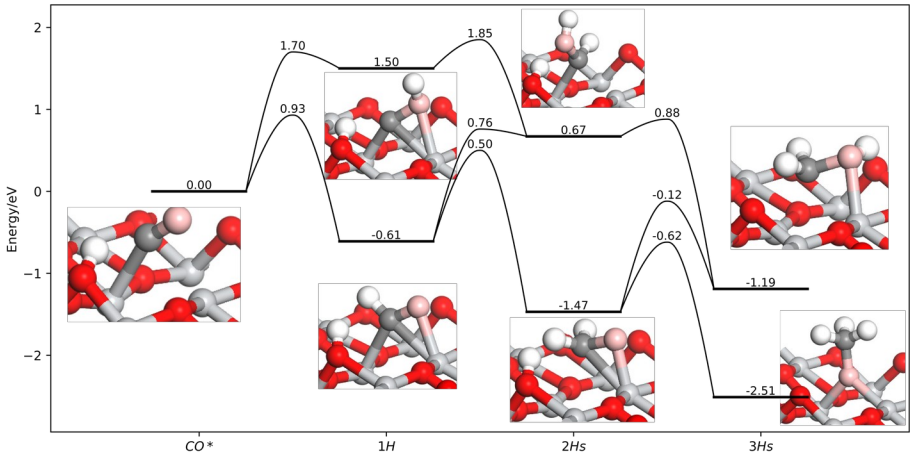

Figure 5. The computed pathways starting from configuration CO(B).

The CO(B) configuration will go through a same transition state as CO(A) → CHO with a barrier of 0.93 eV (Figure 5 and S6 for transition state). Notably, the activation energy of the CO(B) → COH process is 0.5 eV lower than that starting from CO(A). The distance between the O atom of CO(B) and H^+ situated on O_b is 4.0 Å, i.e. large and only marginally smaller than that in the CO(A) pathway (4.13 Å). The more favorable barrier should have to do with the available relay point reported before[42,43]. Even though the distances to H^+ are similar, the O atom in CO(B) is relatively closer to the surface, and the proton can move O_{3c} between Ti^{4+} and Ti^{3+}, the relay point. Thus, hydrogenating the O atom of CO does not require the formation of the H-radical. The barrier of the CO(B) → CHO process is considerably more competitive than even that of the CO(A) → COH process. If the proton binds to C in CO, the subsequent pathways from CHO to CH_3O are downhill for either configuration, and the barriers are 0.89 eV and 0.85 eV, for CO(A) and CO(B) being the starting points, respectively. The CH_2OH intermediate formed from CO(B) is identical to that formed from CO(A). Hence, these two reaction profiles merge in the last hydrogenation step, as shown in Figure 6 and S7.

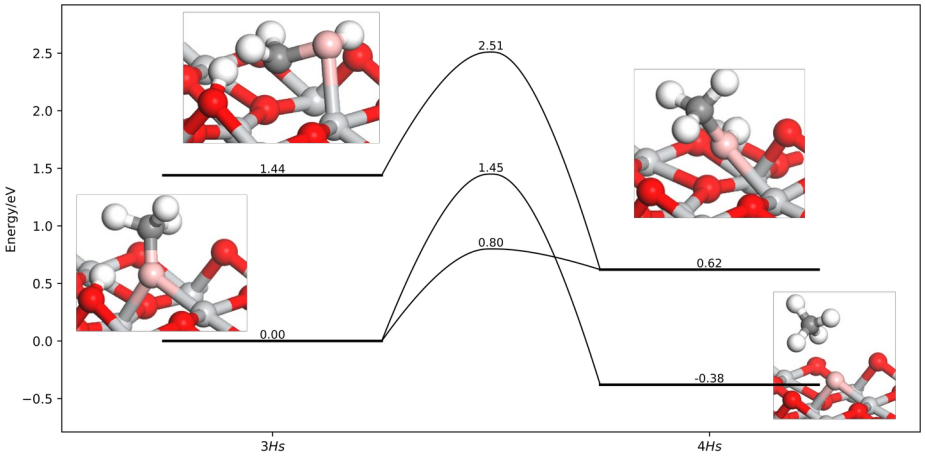

Figure 6. The combined computed pathways leading to methane and methanol

We can see that the CH_2OH intermediate overcomes a barrier of 1.07 eV to form a methanol molecule adsorbed on the O_v site. However, we found the desorption energy for methanol to be as high as 1.66 eV, making it hard for the adsorbate to desorb from O_v at room temperature. Additionally, the barrier from the adsorbed methanol (CH_3OH^*) to CH_3 is quite low (0.18 eV). Therefore, the formation of the CH_3 intermediate is more favorable than the desorption of CH_3OH. The activation energy of 1.45 eV is needed to produce methane from CH_3. The desorption energy of methane is only 0.20 eV, indicating that it can easily escape the surface. The process is quite consistent with the experiment, showing that only CO and CH_4 formed during a room temperature photocatalysis,[14,44] and other theoretical claims[20].
In a conclusion, the overall most favorable pathway from adsorbed CO is CO(A) → CHO → CHOH → CH_2OH → CH_3OH^* → CH_3O → CH_4 or CO(A) → CO(B) → CHO → CH_2O → CH_3O → CH_4. Only CH_4 is expected to be observed at the room temperature as the reaction product. The whole reaction profile is outlined in Figure 7.

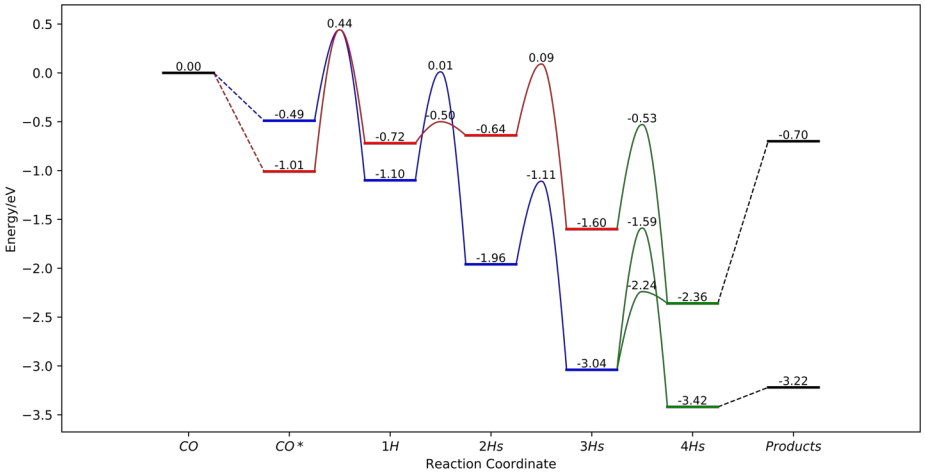

Figure 7. The overall potential energy surface from CO to CH_4. Black, red, blue and green bars and curves represent a desorption state, the most favorable pathway for CO(A), the most favorable pathway for CO(B) and pathways after merged, respectively.

C pathway

Beyond the normal possible pathways of CO, we also found a deoxygenated shortcut to CH_4. Even though Ji et al[20] dismissed this possible mechanism because of the 2.17 eV CO dissociation energy, we nevertheless pursued the search for the possible carbene-like pathway, following the experimental claims.[45] Our calculations indicate that CH can form by dissociation of the CHOH intermediate along the CO(A) pathway, with the activation barrier of 1.96 eV, as shown in Figure 8a and S8. The process is endothermic by 1.74 eV, which is much lower than that reported in Ji's work. The hydroxyl group formed through dissociation is then able to combine with protons on the surface to form water, or with holes to form oxygen molecule leaving the system while protons would stay on the surface to continue the reaction.

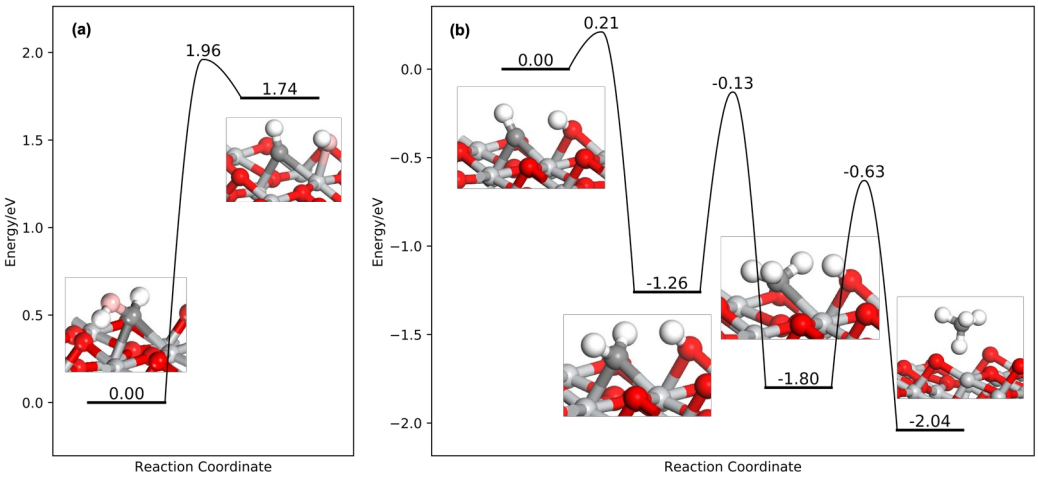

Figure 8. (a) The dissociation of CHOH species on oxygen vacancy site. (b) The pathway from CH to CH_4

As illustrated in Figure 8b, the barrier of the first hydrogenation step is 0.21 eV, which means the CH intermediate can be easily hydrogenated with the first proton. In this configuration, we found that the difference using our correction was as high as 0.42 eV, while involving two extra hydrogens, it became 0.22 eV. When three extra hydrogens introduced, *i.e.* there are CH adsorbate and three H atoms on the defected surface slab, the difference shrink to 0.03 eV, which indicated two extra hydrogens' system should be the initial point in this pathway. This may be attributed to a plenty of electrons were needed to breed a bare carbon to stabilize it. The subsequent hydrogenation steps are downhill, proceeding through a series of steps with the average activation energy of around 1.15 eV, to finally produce methane. Overall, this pathway from CHOH to CH_4 looks thermodynamically quite favorable. Therefore, the direct deoxygenation and hydrogenation pathway is CO_2 → CO(A) → CHO → CHOH → CH → CH_2 → CH_3 → CH_4, where the rate-limiting step is CHOH → CH with a barrier of 1.96 eV.

CONCLUSIONS

We systematically investigated the mechanism of conversion of CO_2 to CH_4 on defected anatase TiO_2 (101) and found that the two most plausible pathways are CO_2 → CO(A)(CO(B)) → CHO(CHO) → $CHOH(CH_2O)$ → $CH_2OH(CH_3O)$ → CH_3OH* or CH_4. The desorption energy of CH_3OH is -1.66 eV, indicating that if it forms, it would be rather stable on the surface at room temperature. Our results suggest that the hydrogenated CO on the O_v site will eventually be reduced to CH_4 in the room temperature in the gas/solid heterogeneous condition. O_v plays a role of activating CO_2 and CO and support intermediates for hydrogen to attack. Beyond that, a hydrocarbon intermediate can be dissociated from the CHOH intermediate, which in formed along the pathway on the O_v site and can go through a downhill pathway reduced into CH_4. It is noteworthy that even though all the pathways from CO_2 are thermodynamically favorable, the barriers between the steps remain high, especially in the carbene-like pathway. Introducing electric field or electrochemical potential may be the way to accelerate the reaction and improve the yield. We will keep focusing on different ways to decrease those high activation energies.

Associated Contents

Supporting Information

The Geometries of transition states and most stable adsorbed CO_2 on pristine slab, charge difference and coordinate files are listed in the supporting information.

Acknowledgments:

Financial support comes from the CSC Fellowship to J.L. and the NSF-CAREER Award CHE-1351968 to A.N.A.. We also acknowledge the UCLA-IDRE cluster Hoffman2 and XSEDE for computational resources.

Reference:

(1) Costentin, C.; Robert, M.; Savéant, J.-M. Catalysis of the Electrochemical Reduction of Carbon Dioxide. *Chem. Soc. Rev.* **2013**, *42*, 2423–2436.

(2) Habisreutinger, S. N.; Schmidt-Mende, L.; Stolarczyk, J. K. Photocatalytic Reduction of CO_2 on TiO_2 and Other Semiconductors. *Angew. Chem. Int. Ed.* **2013**, *52*, 7372–7408.

(3) Corma, A.; Garcia, H. Photocatalytic Reduction of CO_2 for Fuel Production: Possibilities and Challenges. *J. Catal.* **2013**, *308*, 168–175.

(4) Ma, S.; Lan, Y.; Perez, G. M. J.; Moniri, S.; Kenis, P. J. A. Silver Supported on Titania as an Active Catalyst for Electrochemical Carbon Dioxide Reduction. *ChemSusChem.* **2018**, *7*, 866–874.

(5) Yan, Y.; Han, M.; Konkin, A.; Koppe, T.; Wang, D.; Andreu, T.; Chen, G.; Vetter, U.; Morante, J. R.; Schaaf, P. Slightly Hydrogenated TiO_2 with Enhanced Photocatalytic Performance. *J. Mater. Chem. A.* **2014**, *2*, 12708–12716.

(6) Xie, S.; Zhang, Q.; Liu, G.; Wang, Y. Photocatalytic and Photoelectrocatalytic Reduction of CO_2 Using Heterogeneous Catalysts with Controlled Nanostructures. *Chem. Commun.* **2015**, *52*, 35–59.

(7) Chang, X.; Wang, T.; Gong, J. CO_2 Photo-Reduction: Insights into CO_2 Activation and Reaction on Surfaces of Photocatalysts. *Energy Env. Sci.* **2016**, *9*, 2177–2196.

(8) Li, K.; Peng, B.; Peng, T. Recent Advances in Heterogeneous Photocatalytic CO_2 Conversion to Solar Fuels. *ACS Catal.* **2016**, *6*, 7485–7527.

(9) Peng, C.; Reid, G.; Wang, H.; Hu, P. Perspective: Photocatalytic Reduction of CO_2 to Solar Fuels over Semiconductors. *J. Chem. Phys.* **2017**, *147*, 030901.

(10) Inoue, T.; Fujishima, A.; Konishi, S.; Honda, K. Photoelectrocatalytic Reduction of Carbon Dioxide in Aqueous Suspensions of Semiconductor Powders. *Nature* **1979**, *277*, 637–638.

(11) Lee, J.; Sorescu, D. C.; Deng, X. Electron-Induced Dissociation of CO_2 on

TiO_2(110). *J. Am. Chem. Soc.* **2011**, *133*, 10066–10069.
(12) Liu, L.; Zhao, C.; Li, Y. Spontaneous Dissociation of CO_2 to CO on Defective Surface of Cu(I)/TiO2–x Nanoparticles at Room Temperature. *J. Phys. Chem. C* **2012**, *116*, 7904–7912.
(13) Yu, J.; Low, J.; Xiao, W.; Zhou, P.; Jaroniec, M. Enhanced Photocatalytic CO_2-Reduction Activity of Anatase TiO_2 by Coexposed {001} and {101} Facets. *J. Am. Chem. Soc.* **2014**, *136*, 8839–8842.
(14) Liu, L.; Jiang, Y.; Zhao, H.; Chen, J.; Cheng, J.; Yang, K.; Li, Y. Engineering Coexposed {001} and {101} Facets in Oxygen-Deficient TiO_2 Nanocrystals for Enhanced CO_2 Photoreduction under Visible Light. *ACS Catal.* **2016**, *6*, 1097–1108.
(15) He, H.; Zapol, P.; Curtiss, L. A. A Theoretical Study of CO_2 Anions on Anatase (101) Surface. *J. Phys. Chem. C* **2010**, *114*, 21474–21481.
(16) He, H.; Zapol, P.; Curtiss, L. A. Computational Screening of Dopants for Photocatalytic Two-Electron Reduction of CO_2 on Anatase (101) Surfaces. *Energy Environ. Sci.* **2012**, *5*, 6196.
(17) Liu, C.; He, H.; Zapol, P.; Curtiss, L. A. Computational Studies of Electrochemical CO_2 Reduction on Subnanometer Transition Metal Clusters. *Phys Chem Chem Phys* **2014**, *16*, 26584–26599.
(18) Ip, C. M.; Troisi, A. A Computational Study of the Competing Reaction Mechanisms of the Photo-Catalytic Reduction of CO_2 on Anatase(101). *Phys. Chem. Chem. Phys.* **2016**, *18*, 25010–25021.
(19) Ji, Y.; Luo, Y. Theoretical Study on the Mechanism of Photoreduction of CO_2 to CH_4 on the Anatase TiO_2 (101) Surface. *ACS Catal.* **2016**, *6*, 2018–2025.
(20) Ji, Y.; Luo, Y. New Mechanism for Photocatalytic Reduction of CO_2 on the Anatase TiO_2 (101) Surface: The Essential Role of Oxygen Vacancy. *J. Am. Chem. Soc.* **2016**, *138*, 15896–15902.
(21) Diebold, U. The Surface Science of Titanium Dioxide. *Surf. Sci. Rep.* **2003**, *48*, 53–229.
(22) Maity, P.; Mohammed, O. F.; Katsiev, K.; Idriss, H. Study of the Bulk Charge Carrier Dynamics in Anatase and Rutile TiO_2 Single Crystals by Femtosecond Time-Resolved Spectroscopy. *J. Phys. Chem. C* **2018**, *122*, 8925–8932.
(23) Lazzeri, M.; Vittadini, A.; Selloni, A. Structure and Energetics of Stoichiometric TiO_2 Anatase Surfaces. *Phys. Rev. B* **2001**, *63*.
(24) Qiu, J.; Zeng, G.; Ha, M.-A.; Ge, M.; Lin, Y.; Hettick, M.; Hou, B.; Alexandrova, A. N.; Javey, A.; Cronin, S. B. Artificial Photosynthesis on TiO_2 -Passivated InP Nanopillars. *Nano Lett.* **2015**, *15*, 6177–6181.
(25) Qiu, J.; Zeng, G.; Ha, M.-A.; Hou, B.; Mecklenburg, M.; Shi, H.; Alexandrova, A. N.; Cronin, S. B. Microscopic Study of Atomic Layer Deposition of TiO_2 on GaAs and Its Photocatalytic Application. *Chem. Mater.* **2015**, *27*, 7977–7981.
(26) Islam, M. M.; Calatayud, M.; Pacchioni, G. Hydrogen Adsorption and

Diffusion on the Anatase TiO_2(101) Surface: A First-Principles Investigation. *J. Phys. Chem. C* **2011**, *115*, 6809–6814.
(27) Panayotov, D. A.; Yates, J. T. N-Type Doping of TiO_2 with Atomic Hydrogen-Observation of the Production of Conduction Band Electrons by Infrared Spectroscopy. *Chem. Phys. Lett.* **2007**, *436*, 204–208.
(28) Kamat, P. V. Manipulation of Charge Transfer Across Semiconductor Interface. A Criterion That Cannot Be Ignored in Photocatalyst Design. *J. Phys. Chem. Lett.* **2012**, *3*, 663–672.
(29) Kresse, G.; Hafner, J. Ab Initio Molecular Dynamics for Liquid Metals. *Phys. Rev. B* **1993**, *47*, 558–561.
(30) Kresse, G.; Hafner, J. Ab Initio Molecular-Dynamics Simulation of the Liquid-Metal–Amorphous-Semiconductor Transition in Germanium. *Phys. Rev. B* **1994**, *49*, 14251–14269.
(31) Kresse, G.; Furthmüller, J. Efficiency of Ab-Initio Total Energy Calculations for Metals and Semiconductors Using a Plane-Wave Basis Set. *Comput. Mater. Sci.* **1996**, *6*, 15–50.
(32) Kresse, G.; Furthmüller, J. Efficient Iterative Schemes for Ab Initio Total-Energy Calculations Using a Plane-Wave Basis Set. *Phys. Rev. B* **1996**, *54*, 11169–11186.
(33) Blöchl, P. E. Projector Augmented-Wave Method. *Phys. Rev. B* **1994**, *50*, 17953–17979.
(34) Kresse, G.; Joubert, D. From Ultrasoft Pseudopotentials to the Projector Augmented-Wave Method. *Phys. Rev. B* **1999**, *59*, 1758–1775.
(35) Perdew, J. P.; Burke, K.; Ernzerhof, M. Generalized Gradient Approximation Made Simple. *Phys. Rev. Lett.* **1996**, *77*, 3865–3868.
(36) Tkatchenko, A.; Scheffler, M. Accurate Molecular Van Der Waals Interactions from Ground-State Electron Density and Free-Atom Reference Data. *Phys. Rev. Lett.* **2009**, *102*, 073005.
(37) Ha, M.-A.; Alexandrova, A. N. Oxygen Vacancies of Anatase(101): Extreme Sensitivity to the Density Functional Theory Method. *J. Chem. Theory Comput.* **2016**, *12*, 2889–2895.
(38) Tang, W.; Sanville, E. and Henkelman, G. A grid-based Bader analysis algorithm without lattice bias, *J. Phys.: Condens. Matter*, **2009**, 21, 084204
(39) Henkelman, G.; Uberuaga, B. P.; Jónsson, H. A Climbing Image Nudged Elastic Band Method for Finding Saddle Points and Minimum Energy Paths. *J. Chem. Phys.* **2000**, *113*, 9901–9904.
(40) Ko, K. C.; Bromley, S. T.; Lee, J. Y.; Illas, F. Size-Dependent Level Alignment between Rutile and Anatase TiO_2 Nanoparticles: Implications for Photocatalysis. *J. Phys. Chem. Lett.* **2017**, *8*, 5593–5598.
(41) Sorescu, D. C.; Al-Saidi, W. A.; Jordan, K. D. CO_2 Adsorption on TiO_2 (101) Anatase: A Dispersion-Corrected Density Functional Theory Study. *J. Chem. Phys.* **2011**, *135*, 124701.
(42) Kajita, S.; Minato, T.; Kato, H. S.; Kawai, M.; Nakayama, T. First-Principles

Calculations of Hydrogen Diffusion on Rutile TiO_2(110) Surfaces. *J. Chem. Phys.* **2007**, *127*, 104709.

(43) Li, S.-C.; Zhang, Z.; Sheppard, D.; Kay, B. D.; White, J. M.; Du, Y.; Lyubinetsky, I.; Henkelman, G.; Dohnálek, Z. Intrinsic Diffusion of Hydrogen on Rutile TiO2(110). *J. Am. Chem. Soc.* **2008**, *130*, 9080–9088.

(44) Liu, L.; Zhao, H.; Andino, J. M.; Li, Y. Photocatalytic CO_2 Reduction with H_2O on TiO_2 Nanocrystals: Comparison of Anatase, Rutile, and Brookite Polymorphs and Exploration of Surface Chemistry. *ACS Catal.* **2012**, *2*, 1817–1828.

(45) Anpo, M.; Yamashita, H.; Ichihashi, Y.; Ehara, S. Photocatalytic Reduction of CO_2 with H_2O on Various Titanium Oxide Catalysts. *J. Electroanal. Chem.* **1995**, *396*, 21–26.

TOC Graphics: